

7-T ^{35}Cl and ^{23}Na MR Imaging for Detection of Mutation-dependent Alterations in Muscular Edema and Fat Fraction with Sodium and Chloride Concentrations in Muscular Periodic Paralysis¹

Marc-André Weber, MD, MSc
 Armin M. Nagel, PhD
 Anja M. Marschar, MSc
 Philip Glemser, MD
 Karin Jurkat-Rott, MD
 Maya B. Wolf, MD
 Mark E. Ladd, PhD
 Heinz-Peter Schlemmer, MD, PhD
 Hans-Ulrich Kauczor, MD
 Frank Lehmann-Horn, MD, MSc

¹From the Clinic of Diagnostic and Interventional Radiology, University Hospital Heidelberg, Im Neuenheimer Feld 110, D-69120 Heidelberg, Germany (M.A.W., H.U.K.); Department of Radiology (M.A.W., P.G., M.B.W., H.P.S.) and Division of Medical Physics in Radiology (A.M.N., A.M.M., M.E.L.), German Cancer Research Center (DKFZ), Heidelberg, Germany; and Division of Neurophysiology, Ulm University, Ulm, Germany (K.J.R., F.L.H.). From the 2014 RSNA Annual Meeting. Received July 22, 2015; revision requested September 2; revision received January 6, 2016; accepted January 29; final version accepted February 3.

Address correspondence to M.A.W. (e-mail: MarcAndre.Weber@med.uni-heidelberg.de).

A.M.N. supported in part by the Helmholtz Alliance Imaging and Curing Environmental Metabolic Diseases (ICEMED), through the Initiative and Networking Fund of the Helmholtz Association. K.J.R. and M.A.W. supported in part by the Eva Luise Köhler Research Award for Rare Diseases. A.M.M. supported by the Deutsche Forschungsgemeinschaft (DFG), project no. NA736/2-1. K.J.R. and F.L.H. supported in part by research grants from the German Federal Research Ministry (IonNeurOnet), by the German Society for Patients with Muscle Disorders (DGM), and by the nonprofit Hertie Foundation.

© RSNA, 2016

Purpose:

To determine whether altered sodium (Na^+) and chloride (Cl^-) homeostasis can be visualized in periodic paralyzes by using 7-T sodium 23 (^{23}Na) and chlorine 35 (^{35}Cl) magnetic resonance (MR) imaging.

Materials and Methods:

Institutional review board approval and informed consent of all participants were obtained. ^{23}Na (repetition time msec/echo time msec, 160/0.35) and ^{35}Cl (40/0.6) MR imaging of both lower legs was performed with a 7-T whole-body system in patients with genetically confirmed hypokalemic periodic paralysis (Cav1.1-R1239H mutation, $n = 5$; Cav1.1-R528H mutation, $n = 8$) and Andersen-Tawil syndrome ($n = 3$) and in 16 healthy volunteers. Additionally, each participant underwent 3-T proton MR imaging on the same day by using T1-weighted, short-tau inversion-recovery, and Dixon-type sequences. Muscle edema was assessed on short-tau inversion-recovery images, fatty degeneration was assessed on T1-weighted images, and muscular fat fraction was quantified with Dixon-type imaging. Na^+ and Cl^- were quantified in the soleus muscle by using three phantoms that contained 10-, 20-, and 30-mmol/L NaCl solution and 5% agarose gel as a reference. Parametric data for all subpopulations were tested by using one-way analysis of variance with the Dunnett test, and correlations were assessed with the Spearman rank correlation coefficient.

Results:

Median muscular ^{23}Na concentration was higher in patients with Cav1.1-R1239H (34.7 mmol/L, $P < .001$), Cav1.1-R528H (32.0 mmol/L, $P < .001$), and Kir2.1 (24.3 mmol/L, $P = .035$) mutations than in healthy volunteers (19.9 mmol/L). Median muscular normalized ^{35}Cl signal intensity was higher in patients with Cav1.1-R1239H (27.6, $P < .001$) and Cav1.1-R528H (23.6, $P < .001$) than in healthy volunteers (12.6), but not in patients with the Kir2.1 mutation (14.3, $P = .517$). When compared with volunteers, patients with Cav1.1-R1239H and Cav1.1-R528H showed increased muscular edema ($P < .001$ and $P = .003$, respectively) and muscle fat fraction ($P < .001$ and $P = .017$, respectively).

Conclusion:

With 7-T MR imaging, changes of Na^+ and Cl^- homeostasis can be visualized in periodic paralyzes and are most pronounced in the severe phenotype Cav1.1-R1239H, with up to daily paralytic episodes.

© RSNA, 2016

Mutations in muscle ion channels induce a group of rare inherited diseases, the muscle channelopathies (1). These mutations effectuate either an increase or a decrease in muscle membrane excitability, which in turn leads to a variety of related clinical disorders: The delayed relaxation after muscle contraction that causes muscle stiffness and pain characterizes the nondystrophic myotonias; the periodic paralysis are characterized by episodes of flaccid muscle paralysis, with intervals of normal muscle function (1). In the expanding group of muscle channelopathies, the muscle disease is provoked by mutations in calcium, chloride, potassium, and sodium ion channels. These result in decreased or increased muscle membrane excitability caused by altered muscle membrane potential due to changes in ion conductivities. Identifying patients with channelopathies and confirming the diagnosis are crucial, as treatment and management strategies differ on the basis of mutation and clinical phenotype (1). In hypokalemic periodic paralysis (HypoPP), nonselective cation leaks play an important role in causing the paralytic attacks (2). Andersen-Tawil syndrome

(ATS) is rather particular in the spectrum of channelopathies, since it is a multisystem disorder. The full ATS is characterized by periodic paralysis, ventricular arrhythmias, and dysmorphic features (3). Most patients with ATS have a mutation in the ion channel gene *KCNJ2* that encodes the inward rectifier potassium (K⁺) channel Kir2.1. This channel represents a component of the inward rectifier IK1. IK1 that, during the final phase of repolarization, provides repolarizing current (3).

Recently, chlorine 35 (³⁵Cl) magnetic resonance (MR) imaging, together with sodium 23 (²³Na) MR imaging with a 7-T whole-body MR system, could be implemented for evaluating human calf muscles (4). The potential benefit of ²³Na 1.5-T imaging (2) and 3-T imaging (5) in HypoPP has already been demonstrated. Chloride (Cl⁻) is the most abundant and important anion in the human body and is involved in many fundamental physiologic processes. It influences cellular osmolarity and thereby cell volume and regulates cell potential, such as the inhibition of muscular cell excitability (6). Skeletal muscle cells exhibit a very high Cl⁻ conductance, which makes up approximately 80% of the total membrane conductance at rest (7). Thus, the resting membrane potential of muscle cells can be approximated by using the Nernst equation, which only requires the intra- and extracellular Cl⁻ concentrations for calculation (4).

Since, in periodic paralysis, the resting membrane potential is reduced

(7), the objective of our study was to determine whether altered sodium (Na⁺) and Cl⁻ homeostasis can be visualized in these periodic paralysis by using 7-T ²³Na and ³⁵Cl MR imaging.

Materials and Methods

Ethical Policy

Written informed consent was obtained from all participants after the nature of the procedure had been fully explained. Our study was approved by the institutional review board and performed according to the declaration of Helsinki in its present form. No industry gave support specifically for the study. We guarantee that the authors had full control of the data and the information submitted for publication. Moreover, none of the authors is an employee of an industrial company.

Patient Population

Eighteen patients suspected of having periodic paralysis owing to symptoms, medical history (including that of their family members), and findings of clinical examination by an experienced neurologist and physiologist (F.L.H., with 35 years of experience in clinical neurology

Advances in Knowledge

- Median muscular sodium 23 (²³Na) concentration detected with 7-T ²³Na MR imaging was higher in patients with periodic paralysis and Cav1.1-R1239H, Cav1.1-R528H, and Kir2.1 mutations than in healthy volunteers.
- Median muscular normalized chlorine 35 (³⁵Cl) signal intensity (SI) detected with 7-T ³⁵Cl MR imaging was higher in patients with periodic paralysis and Cav1.1-R1239H and Cav1.1-R528H mutations than in healthy volunteers but was not higher in patients with periodic paralysis and Kir2.1 mutation.
- In periodic paralysis, there was a strong correlation between the degree of muscular edema and fat fraction when compared with muscular ²³Na concentration and normalized ³⁵Cl SI.

Implications for Patient Care

- Although 7-T MR imaging technique is currently limited to research applications, 7-T ²³Na and ³⁵Cl MR imaging can be used to monitor ion homeostasis within the skeletal muscle tissue noninvasively.
- When full approval for routine patient care is obtained by the manufacturer, it may help in the testing of pathogenesis, estimating prognosis, and monitoring of treatment in periodic paralysis.

Published online before print

10.1148/radiol.2016151617 Content codes:  

Radiology 2016; 000:1–12

Abbreviations:

ATS = Andersen-Tawil syndrome
HypoPP = hypokalemic periodic paralysis
MRC = British Medical Research Council
ROI = region of interest
SI = signal intensity
STIR = short-tau inversion recovery

Author contributions:

Guarantors of integrity of entire study, M.A.W., H.P.S.; study concepts/study design or data acquisition or data analysis/interpretation, all authors; manuscript drafting or manuscript revision for important intellectual content, all authors; approval of final version of submitted manuscript, all authors; agrees to ensure any questions related to the work are appropriately resolved, all authors; literature research, M.A.W., A.M.N., P.G., M.E.L.; clinical studies, M.A.W., A.M.N., K.J.R., F.L.H.; experimental studies, M.A.W., A.M.N., A.M.M., K.J.R.; statistical analysis, M.A.W.; and manuscript editing, all authors

Conflicts of interest are listed at the end of this article.

and muscle diseases) were prospectively included in our study from October 2012 until February 2015. Further inclusion criteria were willingness to support the research and availability on the days of the MR imaging time slots on weekends. There were no clinical criteria for exclusion (except for missing informed consent and typical MR imaging contraindications, such as cochlear implants and pacemakers) so that the participating subgroup represents a typical patient population of these rare diseases.

To confirm mutations typical of HypoPP or ATS, whole blood (20 mL from each patient) anticoagulated in ethylenediaminetetraacetic acid was used for mutation analysis. Mutation screening was performed by two experienced physiologists (K.J.R., F.L.H.) by using polymerase chain reaction amplification. Polymerase chain reaction products were loaded on 2% agarose gel and stained with ethidium bromide, and the band was cut out under ultraviolet light. Bands were purified and cycle-sequenced with 1 pmol of primer by using the dye terminator kit (Applied Biosystems, Foster City, Calif). The exons and exon-intron boundaries of CACNA1S and KCNJ2 were amplified from genomic DNA and bidirectionally sequenced on 6% denaturing polyacrylamide gels by using an automated 373A sequencer (Applied Biosystems). All sequences with base exchanges were verified with reverse sequencing of a new

polymerase chain reaction product of the same DNA sample.

In 13 patients (seven women [median age, 44 years; range, 28–66 years] and six men [median age, 48 years; range, 40–69 years]), HypoPP was genetically confirmed. There was no significant difference in age between men and women ($P = .64$). Five patients had the severe phenotype Cav1.1-R1239H mutation (one man, four women; median age, 44 years), and eight had the mild phenotype Cav1.1-R528H mutation (five men, three women; median age, 48 years). In three patients, ATS was genetically confirmed (two women with the G215R mutation, one man with the R82 W mutation; median age, 46 years). In two patients suspected of having periodic paralysis (one woman, one man; median age, 62 years), a mutation could not be verified until present. For comparison and for optimization of the MR imaging protocol prior to

patient enrollment, 16 healthy volunteers were included (eight men, eight women; median age, 27 years; range 18–73 years). None of the volunteers in the control group showed any evidence of muscular or cardiovascular disorders, and all volunteers exhibited full muscle strength at physical examination.

3-T MR Imaging Examination and Analysis

Each patient and volunteer underwent 3-T proton MR imaging (Magnetom Trio; Siemens, Erlangen, Germany) on the same day as the 7-T examination of both lower legs by using axial T1-weighted (repetition time msec/echo time msec, 700/10; section thickness, 3 mm), short-tau inversion-recovery (STIR; 5690/66; section thickness, 3 mm), and axial two-point Dixon-type (multiecho chemical-shift–encoded water-fat imaging; 50/2.46 and 3.69; section thickness, 4 mm) sequences (Tables 1, 2). Muscle edema

Table 1

Parameters for 3-T MR Imaging Sequences

3-T ¹ H Imaging Sequence	Repetition Time (msec)	Echo Time (msec)	Flip Angle (degrees)	Resolution (mm)	Imaging Time
T1-weighted turbo spin-echo	700	10	130	0.78 × 0.78 × 3	3 min 0 sec
STIR (inversion time, 220 msec)	5690	66	150	0.68 × 0.68 × 3	1 min 43 sec
Two-point gradient-echo Dixon-type	50	2.46, 3.69	5	0.91 × 0.91 × 4	2 min 47 sec

Table 2

Parameters for 7-T MR Imaging Sequences

7-T ²³ Na and ³⁵ Cl Imaging Sequence	Repetition Time (msec)	Echo Time (msec)	Flip Angle (degrees)	No. of Signals Acquired	No. of Projections	Nominal Isotropic Resolution (mm)	Imaging Time
Sequence A, sodium concentration 3D radial density–adapted	160	0.35	90	1	4000	4 × 4 × 4	10 min 40 sec
Sequence B, sodium B ₁ 3D radial density–adapted	93	0.35	45	1	4000	4 × 4 × 4	06 min 12 sec
Sequence C, sodium B ₀ 3D radial density–adapted	93	1.35	45	1	4000	4 × 4 × 4	06 min 12 sec
Sequence D, chlorine MR imaging 3D radial density–adapted	40	0.6	90	5	5000	12 × 12 × 12	16 min 40 sec

Note.—To reduce Gibbs ringing artifacts, a Hamming filter was applied for ²³Na and ³⁵Cl MR imaging. The sodium concentration maps were corrected for B₀ and B₁ inhomogeneities. The double flip angle method (8) and pulse sequences A and B were used to derive the required B₁ maps. To correct for B₀ inhomogeneities, the data set with the echo times of 0.35 msec (sequence B) and 1.35 msec (sequence C) were used to calculate off-resonance values (B₀ maps). Then the data sets were reconstructed multiple times with the corresponding off-resonance values for each pixel to correct for B₀ inhomogeneities. 3D = three-dimensional.

Figure 1

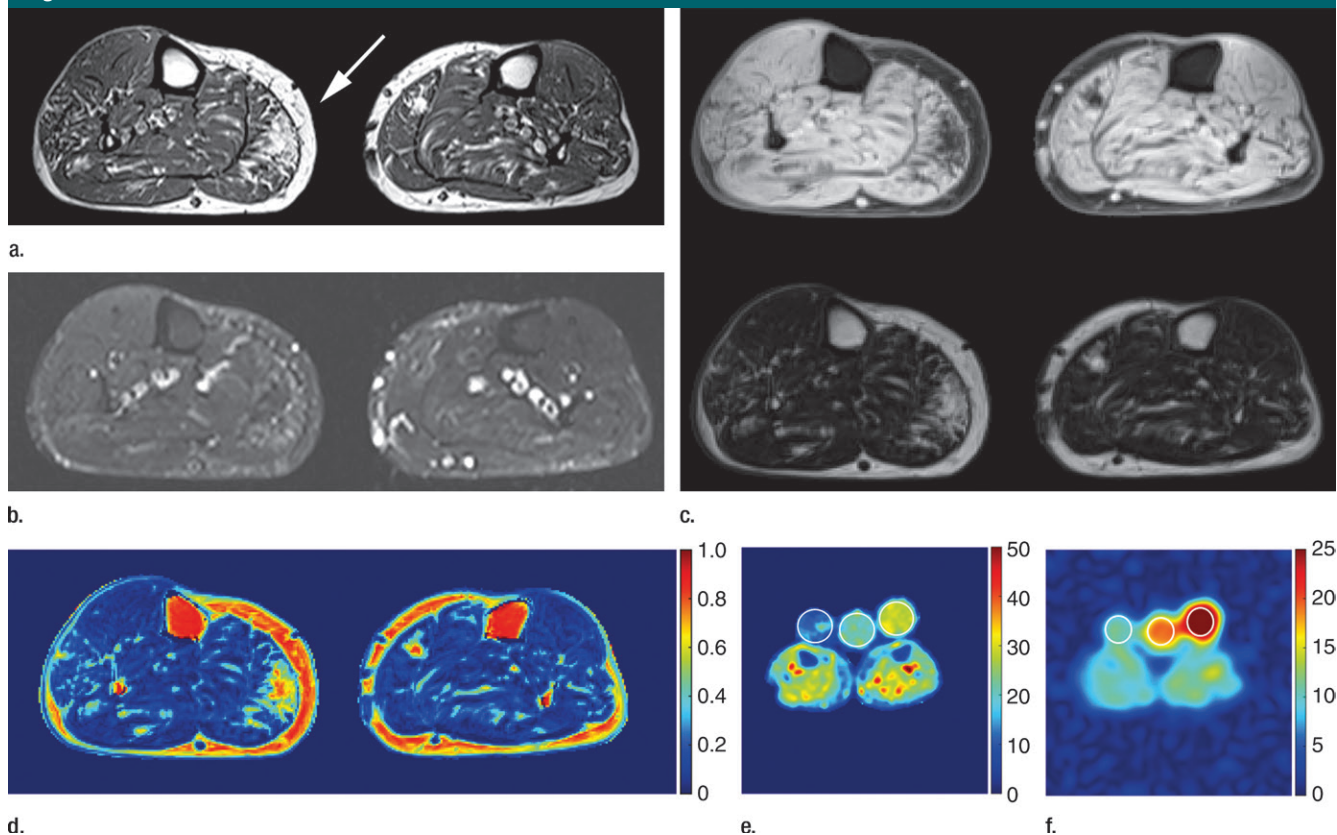


Figure 1: Illustration of MR imaging findings in (a–f) a 66-year-old female patient with HypoPP (with the Cav1.1-R1239H mutation) versus (g–l) a 21-year-old male healthy volunteer. Axial (a, g) 3-T ^1H T1-weighted MR images (700/10) of both calves are shown, with (b, h) STIR images (5690/66), (c, i) water and fat images obtained with the Dixon-type sequence (50/2.46 and 3.69), (d, j) fat fraction maps obtained by using the Dixon-type sequence, (e, k) 7-T ^{23}Na MR images (160/0.35), and (Fig 1 continues.)

was assessed on STIR images, fatty degeneration was assessed on T1-weighted images, and muscular fat fraction was quantified by using Dixon-type imaging. Areas of signal intensity (SI) equivalent to the signal received from subcutaneous fat on T1-weighted hydrogen 1 (^1H) MR images were interpreted as fatty infiltration caused by chronic myopathy. One reader (M.A.W.) with 15 years of experience in musculoskeletal MR imaging scored the lipomatous degeneration with a four-point semiquantitative visual scale, as described previously (9,10). This scale is used to rate the intramuscular fat by using the intensity of subcutaneous fat as a reference and has been shown to correlate well with ratings assigned via automated computer analysis (9). Examined calf muscles included the tibialis anterior

compartment, the soleus, the medial and lateral gastrocnemius, and the peroneal and the deep posterior compartment muscles. Grade 1 was assigned for homogeneous hypointensity, contrasting sharply with subcutaneous and intermuscular fat (normal muscle). Grade 2 was assigned for slight hyperintensity, with patchy intramuscular SI changes. Grade 3 was assigned for marked hyperintensity with patchy but widespread intramuscular SI changes. Grade 4 was assigned for homogeneous hyperintensity in the whole muscle, similar to the SI of adjacent subcutaneous or paramuscular fat.

We defined areas of localized hyperintensity on STIR MR images as muscular edema-like changes according to Marden et al (11). We evaluated the presence of this criterion with a

four-point semiquantitative visual scale, as has been described previously (10). Grade 1 was assigned for homogeneous hypointensity, contrasting sharply with subcutaneous and intermuscular fat (normal muscle, no edema). Grade 2 was assigned for slight hyperintensity with patchy intramuscular SI changes on STIR images (<50% of muscle cross-sectional area). Grade 3 was assigned for marked hyperintensity with patchy but widespread intramuscular SI changes on STIR images (>50% of muscle cross-sectional area). Grade 4 was assigned for homogeneous hyperintensity in whole muscle on STIR images (100% of muscle cross-sectional area).

Besides the qualitative image analysis, the same reader (M.A.W.)

Figure 1 (continued)

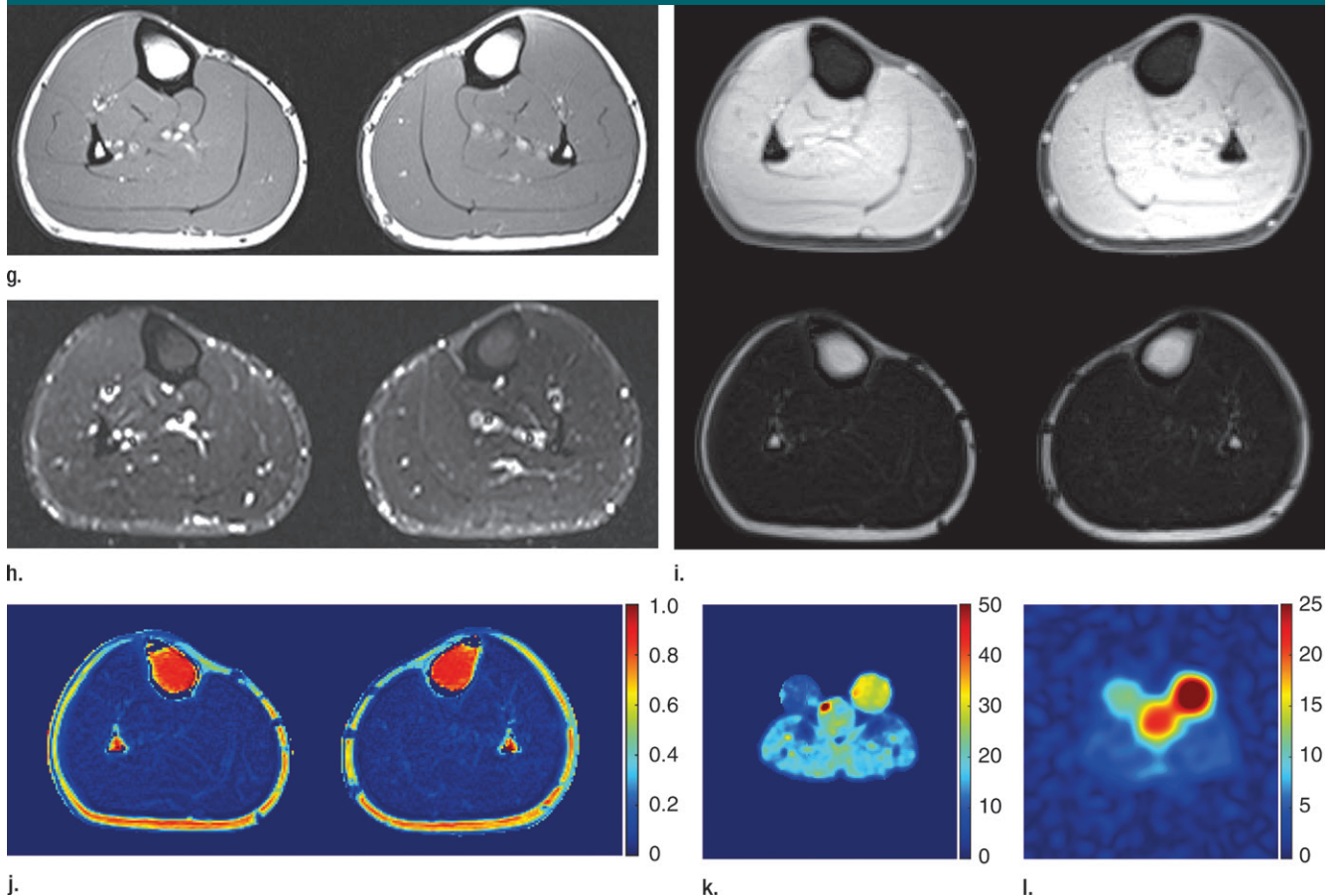


Figure 1 (continued): (f, i) ^{35}Cl MR images (40/0.6). The Na^+ and Cl^- color bars are scaled differently (by a factor of two). Fatty changes in the medial head of the gastrocnemius muscle are most pronounced on the right side (arrow on a) and are only visible in the patient with HypoPP. The higher muscular ^{23}Na and ^{35}Cl SIs in the calf muscles of the patient with HypoPP (with the Cav1.1-R1239H mutation) are evident when compared with those in the healthy control subject. Three reference phantoms that contained 5% agarose gel and 10-, 20-, or 30-mmol/L NaCl solutions were used for signal normalization. ROIs were placed in each reference phantom, and linear regression was performed to quantify Na^+ concentration and to derive normalized SIs for ^{35}Cl MR images. Note that the fast transverse relaxation of ^{35}Cl prevents quantitative determinations of Cl^- concentrations. In the ROIs of the three reference tubes (e), the measured Na^+ concentrations are $9.8 \text{ mmol/L} \pm 3.6$, $20.6 \text{ mmol/L} \pm 1.9$, and $29.6 \text{ mmol/L} \pm 1.6$. For ^{35}Cl MR imaging (f), the normalized SIs in the three ROIs are 10.7 ± 0.5 , 19.0 ± 0.6 , and 29.6 ± 1.3 .

quantified the lipomatous degeneration of the soleus muscle on T1-weighted images according to the ratio of SI of muscle and subcutaneous fat tissue as a reference by using region of interest (ROI) analysis ($\text{ROI}_{\text{muscle}}/\text{ROI}_{\text{subcutaneous fat}}$), according to the method of Jurkat-Rott et al (2) in the same sections. Moreover, the reader also semiquantitatively assessed edema-like changes of the soleus muscle on STIR images as has been described previously (2,10) by using ROI analysis with background noise as reference ($\text{ROI}_{\text{muscle}}/\text{ROI}_{\text{background noise}}$). We used the mean

of the respective ratios for statistical analysis.

Additionally, the fat fraction was calculated by using the Dixon-type images (Fig 1). The radiologist (M.A.W.) with 15 years of experience in musculoskeletal MR imaging analyzed the MR images by positioning ROIs on different muscles of the participant's lower leg (w in the following equation) and fat (f in the following equation) images, the fat fraction (ff in the following equation) was calculated as follows: $ff = f/(f + w)$.

7-T MR Imaging Examination and Analysis

The ^{23}Na and ^{35}Cl examinations were performed with a 7-T whole-body system (Magnetom 7T; Siemens, Erlangen, Germany) on the same day as the 3-T examinations. The 7-T whole-body system was equipped with a double-resonant ($^{35}\text{Cl}/^{23}\text{Na}$) birdcage coil (RAPID Biomedical, Rimpar, Germany) with the following frequencies: ^{35}Cl , 29.1 MHz; and ^{23}Na , 78.6 MHz (12). Principal features of the sequences used for Na^+ and Cl^- concentration measurements in the calf muscles have been described previously in detail (4,13). In short, we used

a three-dimensional density-adapted projection reconstruction sequence (13) for ²³Na MR imaging (160/0.35; section thickness, 4 mm) and ³⁵Cl MR imaging (40/0.6; section thickness, 4 mm) with minimized T2* relaxation weighting (Table 2). The 7-T ³⁵Cl and ²³Na MR imaging was performed without repositioning the patient. Na⁺ concentrations and Cl⁻ normalized SIs were quantified in the soleus muscle by using three phantoms as a reference that contained 5% agarose gel and 10-, 20-, or 30-mmol/L NaCl solutions. For exact positioning of ROIs within the soleus muscles, the 3-T ¹H MR images were used as a reference. When distinct lipomatous degeneration of certain muscles was observed on the 3-T ¹H MR images, the reader (M.A.W.) positioned ROIs in an area with more intact muscle. For normalization, supplementary ROIs were placed on the reference phantoms.

Muscle Strength Grading

The same physician (F.L.H.) quantified muscle strength of all patients and volunteers immediately after the MR imaging examination by using the nonlinear grading system defined by the British Medical Research Council (MRC) (14). He assessed the strength of foot dorsiflexion and plantar flexion and hip and knee flexion and extension.

Data Analysis and Statistics

Results were expressed as means ± standard deviations for quantitative data and as medians and ranges for the MRC scale results. Descriptive statistics were provided where appropriate. Parametric data (eg, muscular Na⁺ and Cl⁻ SI, as well as muscular edema, fatty degeneration, and fat fraction) for all subpopulations were tested by using one-way analysis of variance with the Dunnett test. Correlations between muscular edema, fatty degeneration, fat fraction, Na⁺ concentration, and normalized ³⁵Cl SI were assessed by using the Spearman rank correlation coefficient. Normality of data was tested according to the Shapiro-Wilk test. In all statistical tests, an effect was considered to be statistically significant if the *P* value was less than

Table 3

Pattern of Fatty Muscular Infiltration

Muscle Group and Side	Patients with Kir2.1	Patients with Cav1.1-R528H	Patients with Cav1.1-R1239H	Healthy Volunteers
Tibialis anterior compartment				
Right	1 (1–1)	1 (1–1)	1 (1–1)	1 (1–1)
Left	1 (1–1)	1 (1–1)	1 (1–1)	1 (1–1)
Peroneal muscles				
Right	1 (1–1)	1 (1–2)	2 (1–2)	1 (1–1)
Left	1 (1–1)	1 (1–2)	2 (1–2)	1 (1–1)
Deep posterior compartment				
Right	1 (1–1)	1 (1–2)	1 (1–2)	1 (1–1)
Left	1 (1–1)	1 (1–2)	1 (1–2)	1 (1–1)
Soleus				
Right	1 (1–2)	1.5 (1–3)	2 (1–3)	1 (1–2)
Left	1 (1–2)	1.5 (1–3)	2 (1–3)	1 (1–2)
Medial gastrocnemius				
Right	1 (1–2)	2 (1–3)	3 (2–3)	1 (1–2)
Left	1 (1–2)	2 (1–3)	3 (2–3)	1 (1–1)
Lateral gastrocnemius				
Right	1 (1–1)	1 (1–4)	2 (2–4)	1 (1–1)
Left	1 (1–1)	1 (1–4)	2 (1–4)	1 (1–1)

Note.—Data are medians, with ranges (minimum to maximum values) in parentheses. Fatty infiltration of the musculature was qualitatively assessed with a four-point visual scale, as described in Materials and Methods (9,10) (grade 1, normal muscle; grade 2, slight hyperintensity with patchy intramuscular SI changes; grade 3, marked hyperintensity with patchy but widespread intramuscular SI changes; and grade 4, homogeneous hyperintensity in whole muscle, similar to the SI of adjacent subcutaneous or paramuscular fat). In the oldest volunteer, a 73-year-old man, grade 2 fatty infiltration was observed in both soleus muscles.

.05. *P* values were not adjusted for multiple testing, and the interpretation of *P* values was explorative, given the pilot character of our study. Data entry procedures and statistical evaluation were performed with SPSS software version 18 (SPSS, Somers, NY).

Results

3-T MR Imaging Examination and Analysis

Fatty muscle infiltration was observed on T1-weighted images in all five patients with HypoPP and the severe phenotype Cav1.1-R1239H, in six of eight patients with the mild HypoPP phenotype Cav1.1-R528H, and in one of three patients with ATS (Kir2.1 mutation). Fatty muscle infiltration was absent in the two patients suspected of having periodic paralysis but who did not have mutation verification. Mainly, the medial head of the gastrocnemius muscle was affected, whereas the tibialis

anterior and deep posterior compartments were spared (Table 3). Also, muscle edema was present on STIR images in all five patients with HypoPP with the severe phenotype Cav1.1-R1239H, where mainly the soleus and medial gastrocnemius muscles were affected. Muscle edema was also present in five of eight patients with the mild HypoPP phenotype Cav1.1-R528H but was absent in all patients with ATS (Table 4) and in the two patients without mutation verification. The median score for edema-like and fatty changes of all lower leg muscles of the volunteers at qualitative analysis was 1 (ie, normal muscle tissue). The pattern of lipomatous muscular degeneration (Table 3) and edema-like muscular changes (Table 4) was mostly symmetrical in both lower legs.

At semiquantitative analysis, when compared with volunteers (10.7 ± 2.1), patients with Cav1.1-R1239H (27.4 ± 14.7, *P* < .001) and Cav1.1-R528H (22.7 ± 6.9, *P* = .003) showed

Table 4

Pattern of Edema-like Muscular Changes

Muscle Group and Side	Patients with Kir2.1	Patients with Cav1.1-R528H	Patients with Cav1.1-R1239H	Healthy Volunteers
Tibialis anterior compartment				
Right	1 (1-1)	1 (1-1)	2 (1-2)	1 (1-1)
Left	1 (1-1)	1 (1-1)	2 (1-2)	1 (1-1)
Peroneal muscles				
Right	1 (1-1)	1 (1-1)	2 (1-4)	1 (1-1)
Left	1 (1-1)	1 (1-1)	2 (1-3)	1 (1-1)
Deep posterior compartment				
Right	1 (1-1)	1 (1-2)	2 (1-3)	1 (1-1)
Left	1 (1-1)	1 (1-2)	2 (1-2)	1 (1-1)
Soleus				
Right	1 (1-1)	2 (1-3)	4 (1-4)	1 (1-1)
Left	1 (1-1)	1.5 (1-3)	4 (1-4)	1 (1-1)
Medial gastrocnemius				
Right	1 (1-1)	1 (1-4)	3 (1-4)	1 (1-2)
Left	1 (1-1)	1 (1-4)	3 (1-4)	1 (1-1)
Lateral gastrocnemius				
Right	1 (1-1)	1 (1-3)	1 (1-4)	1 (1-1)
Left	1 (1-1)	1 (1-3)	1 (1-4)	1 (1-2)

Note.—Data are medians, with ranges (minimum to maximum values) in parentheses. Edema-like muscular changes were qualitatively assessed on a four-point visual scale as described in Materials and Methods (10) (grade 1, normal muscle, no edema; grade 2, slight hyperintensity with patchy intramuscular SI changes on STIR images; grade 3, marked hyperintensity with patchy but widespread intramuscular SI changes on STIR images; and grade 4, homogeneous hyperintensity in whole muscle on STIR images).

increased normalized muscular SI on STIR images. When compared with patients with ATS (13.3 ± 2.2), only patients with Cav1.1-R1239H had a higher degree of muscular edema ($P = .031$). Patients with Cav1.1-R1239H and Cav1.1-R528H mutations had fatty muscle degeneration with a mean fat fraction of 0.41 ± 0.30 ($P < .001$) and 0.15 ± 0.11 ($P = .017$) when compared with volunteers (0.06 ± 0.02). However, in Kir2.1 mutations, fat fraction was not increased (0.07 ± 0.01 , $P = .770$). In addition, the muscular fat content was highest in Cav1.1-R1239H mutations with an SI ratio of muscle in relation to subcutaneous fat tissue of 0.57 ± 0.19 on T1-weighted images and was significantly increased when compared with volunteers (0.35 ± 0.04 , $P < .001$). Also, this SI ratio was significantly increased in patients with the Cav1.1-R528H mutation (0.46 ± 0.08 , $P = .027$) but not in patients with the Kir2.1 mutation (0.43 ± 0.08 , $P = .463$) when compared with volunteers.

Compared with healthy volunteers, the two patients suspected of having periodic paralysis without mutation verification showed increased normalized muscular SI on STIR images (19.6 ± 6.5 , $P < .001$), higher fat fraction (0.09 ± 0.01 , $P = .016$), and higher SI ratio of muscle in relation to subcutaneous fat tissue on T1-weighted images (0.41 ± 0.06 , $P = .038$).

7-T MR Imaging Examination and Analysis

Figures 1 and 2 show typical MR images in HypoPP (Cav1.1-R1239H and Cav1.1-R528H mutation) and ATS. Mean muscular ²³Na concentration was higher in patients with Cav1.1-R1239H ($35.3 \text{ mmol/L} \pm 9.2$, $P < .001$), Cav1.1-R528H ($33.0 \text{ mmol/L} \pm 3.9$, $P < .001$), and Kir2.1 ($24.3 \text{ mmol/L} \pm 0.8$, $P = .035$) mutation than in healthy volunteers ($19.9 \text{ mmol/L} \pm 1.9$). The mean muscular normalized ³⁵Cl SI was higher in patients with Cav1.1-R1239H (25.3 ± 8.5 , $P < .001$) and Cav1.1-R528H

(22.9 ± 3.6 , $P < .001$) than in healthy volunteers (12.2 ± 1.6) but was not higher in patients with the Kir2.1 mutation (14.3 ± 1.9 , $P = .517$). When compared with healthy volunteers, the two patients suspected of having periodic paralysis without mutation verification showed increased muscular ²³Na concentration ($25.8 \text{ mmol/L} \pm 1.8$, $P = .23$) and normalized ³⁵Cl SI (20.7 ± 6.3 , $P = .21$). When the results were pooled for all patients, median muscular ²³Na concentration ($P < .001$), ³⁵Cl SI ($P < .001$), muscular edema ($P < .001$), fatty muscular degeneration ($P = .001$), and fat fraction ($P = .035$) were higher in patients than in control subjects.

There was a strong correlation between the degree of muscular edema and muscular ²³Na concentration ($\rho = 0.828$, $P < .001$) and muscular normalized ³⁵Cl SI ($\rho = 0.852$, $P < .001$). Also, there was a strong correlation between the degree of fatty muscular degeneration and muscular ²³Na concentration ($\rho = 0.644$, $P < .001$) and muscular normalized ³⁵Cl SI ($\rho = 0.727$, $P < .001$). In addition, there was a strong correlation between muscular ²³Na concentration and muscular normalized ³⁵Cl SI ($\rho = 0.896$, $P < .001$; Fig 3) and between the degree of fatty muscular degeneration and muscular edema ($\rho = 0.788$, $P < .001$). Moreover, there was a strong correlation between the muscular fat fraction and muscular ²³Na concentration ($\rho = 0.845$, $P < .001$), muscular normalized ³⁵Cl SI ($\rho = 0.892$, $P = .001$), and fatty muscular degeneration as assessed on T1-weighted images ($\rho = 0.624$, $P = .001$), as well as a strong correlation between the muscular fat fraction and muscular edema ($\rho = 0.798$, $P < .001$).

Muscle Strength Grading

Permanent muscle weakness as assessed with the MRC scale was most pronounced in the severe phenotype Cav1.1-R1239H (five of five patients) compared with Cav1.1-R528H (one of eight patients) and in patients suspected of having periodic paralysis without mutation verification (one of two patients). Permanent muscle weakness as assessed with the MRC scale

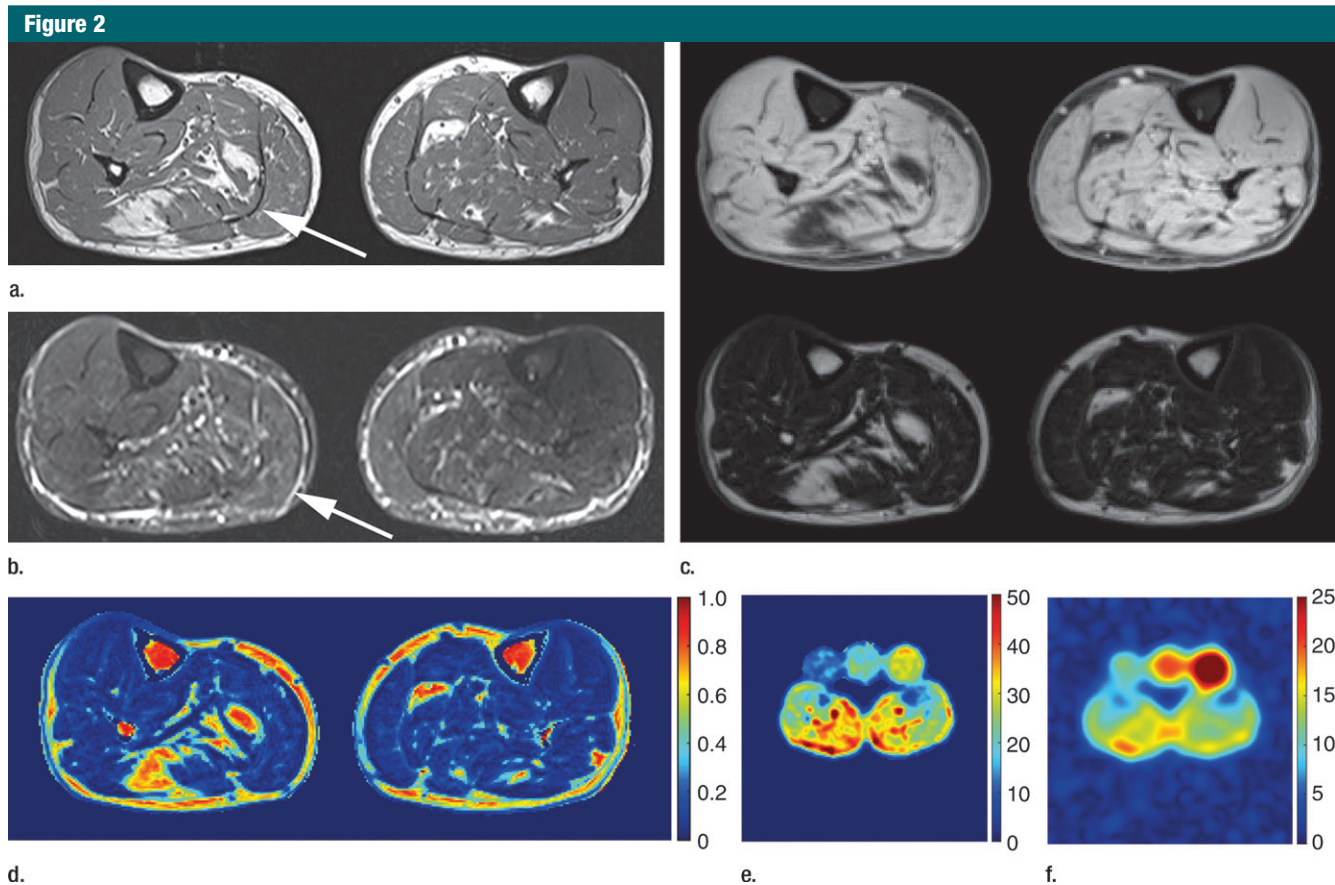


Figure 2: Illustration of MR imaging findings in (a–f) a 69-year-old male patient with HypoPP (mild phenotype, Cav1.1-R528H) compared with (g–l) a 19-year-old female patient with ATS. Axial (a, g) 3-T ^1H T1-weighted MR images (700/10) of both calves are shown, with (b, h) STIR images (5690/66), (c, i) water and fat images obtained by using the Dixon-type sequence (50/2.46 and 3.69), (d, j) fat fraction maps obtained by using the Dixon-type sequence, (e, k) 7-T ^{23}Na MR images (160/0.35), and (Fig 2 continues.)

was absent in patients with ATS and in healthy volunteers. The muscle weakness was mostly symmetrical (Table 5).

Discussion

As demonstrated in our study, changes of Na^+ and Cl^- homeostasis are quantifiable in periodic paralyses by using 7-T MR imaging. These changes are most pronounced in the patients with severe phenotype Cav1.1-R1239H, with up to daily paralytic episodes. Our findings are a step forward into the noninvasive measurement of electrophysiological parameters such as the resting membrane potential of skeletal muscle cells by using MR imaging. Moreover, the visualization of pathophysiological processes provoked by altered Na^+ and Cl^-

channels has become possible with the implemented 7-T MR imaging protocol. The findings of our study substantiate reports on 1.5-T ^{23}Na MR imaging that demonstrated an increased Na^+ concentration of the skeletal muscle tissue in HypoPP (2). Also, our findings substantiate an initial report on two patients with HypoPP who had permanent weakness due to a sustained membrane depolarization at presentation and increased muscular Cl^- concentration (4). Because this reduced membrane potential reflects Cl^- concentration within the skeletal muscle tissue, as demonstrated in our study for both HypoPP mutations in comparison with healthy volunteers, was expected. The measured Cl^- and Na^+ concentration of

normal skeletal muscle tissue was in accordance with recent reports (4).

As described by Nguyen et al (15), ATS is a rare hereditary multisystem disorder with periodic paralysis, ventricular arrhythmias, and dysmorphic features as the typical triad of symptoms. However, the expressivity of the aforementioned symptoms varies distinctly, even within single families affected by ATS. Furthermore, not all patients with ATS present with the full triad of symptoms (15). The syndrome is associated with a loss-of-function mutation in the *KCNJ2* gene. This gene encodes the Kir2.1 inward rectifier K^+ channel. In ATS, the loss-of-function mutations in *KCNJ2* affect the excitability of both skeletal and cardiac muscle, which forms the basis of the

Figure 2 (continued)

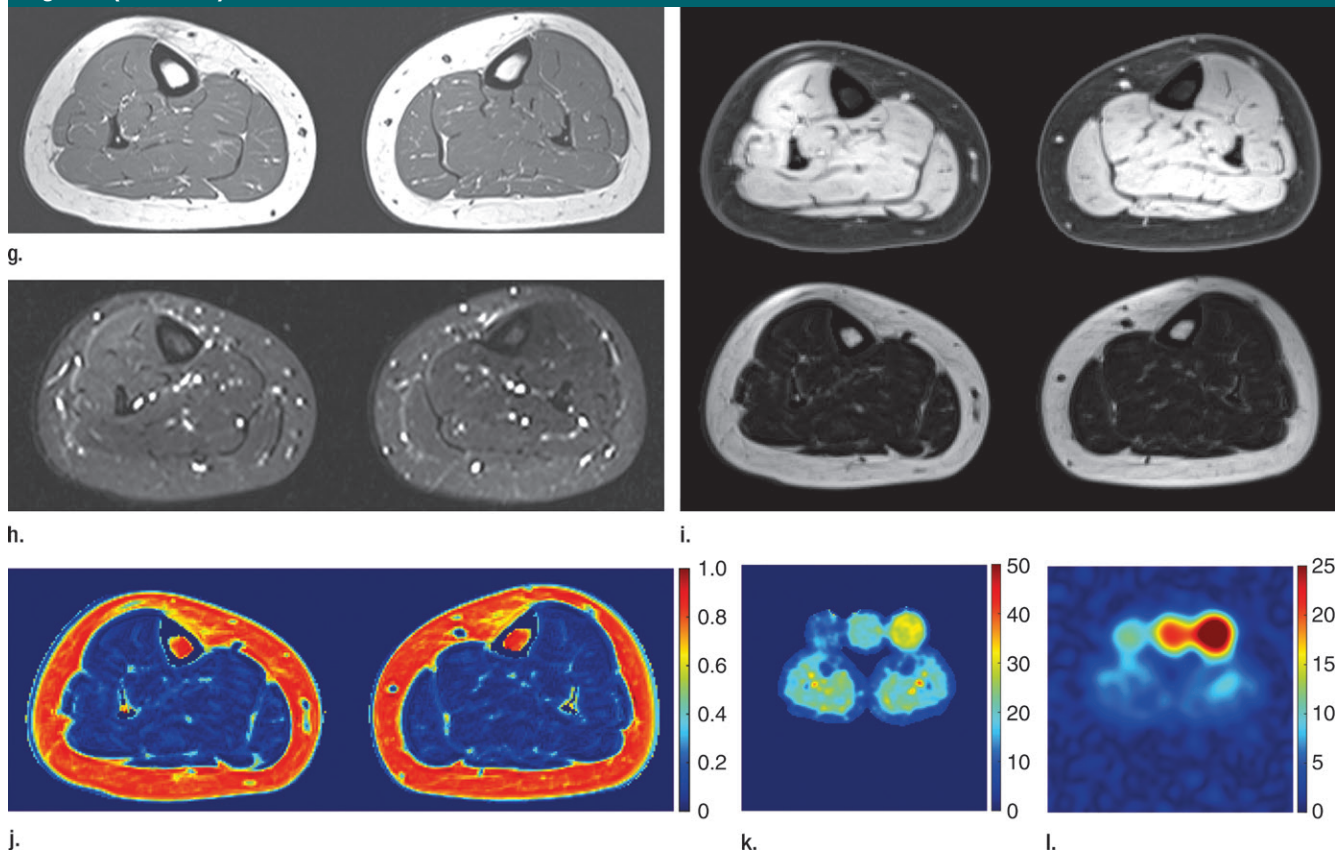


Figure 2 (continued): (f, i) ^{35}Cl MR images (40/0.6). The Na^+ and Cl^- color bars are scaled differently (by a factor of two). The higher muscular ^{23}Na and ^{35}Cl SIs are evident in the calf muscles in the patient with HypoPP when compared with those in the patient with ATS. The tibial bones exhibit low ^{23}Na SI. The three reference phantoms that contained 5% agarose gel and 10-, 20-, or 30-mmol/L NaCl solutions are visible on top of the calves. While edema-like and lipomatous changes are evident mainly in the right soleus muscle of the patient with HypoPP (arrows on **a** and **b**), they are completely absent in the patient with ATS.

periodic paralysis and cardiac arrhythmias associated with ATS (15). Until now, the molecular mechanism of the dysmorphic features in ATS has only been poorly understood. In our study, we observed that the Na^+ concentration within the skeletal muscle tissue is increased in both patients with HypoPP and those with ATS when compared with healthy volunteers. Consequentially, one may hypothesize that the observed muscular Na^+ overload in the studied periodic paralyses HypoPP and ATS may be part of a general mechanism in muscular degeneration, which in other muscular diseases such as muscular dystrophies has also been hypothesized to be a contributor to the progressive muscle degeneration (10). The permanent myoplasmic Na^+

overload may also play a role in the development of the muscle edema, which was present in all patients with HypoPP studied with the severe phenotype. The edema-like changes we observed in HypoPP were in accordance with a previous report (2). The muscular edema we examined seemed to be of an osmotic nature and was mainly intracellular in patients with HypoPP who exhibit myoplasmic Na^+ overload, muscular edema (2), and Cl^- overload (4)—all of which, when persisting, may lead to weakness and degeneration, especially in the severe phenotype Cav1.1-R1239H. Our findings of a strong correlation between the degree of muscular edema and fatty muscular degeneration with the muscular ^{23}Na concentration and muscular normalized ^{35}Cl SI substantiate this

hypothesis. This myocellular accumulation of ions is obviously caused by the membrane leakage due to an aberrant pore in the voltage sensor in HypoPP (2). In brain infarction, increased ^{35}Cl and ^{23}Na SI has been reported in rats, thus substantiating the link between ion overload and cell damage (16,17). Moreover, an increased Cl^- concentration has been reported in glioma tissue of humans by using 7-T MR imaging (4) and in rats by using 21.1 T (18), substantiating the hypothesis of the importance of Cl^- for tumor cell function and progression.

Our study had a few limitations. We acknowledge the preliminary nature and limited generalizability of our findings as a limitation, given the low number of participants. However, all

Figure 3

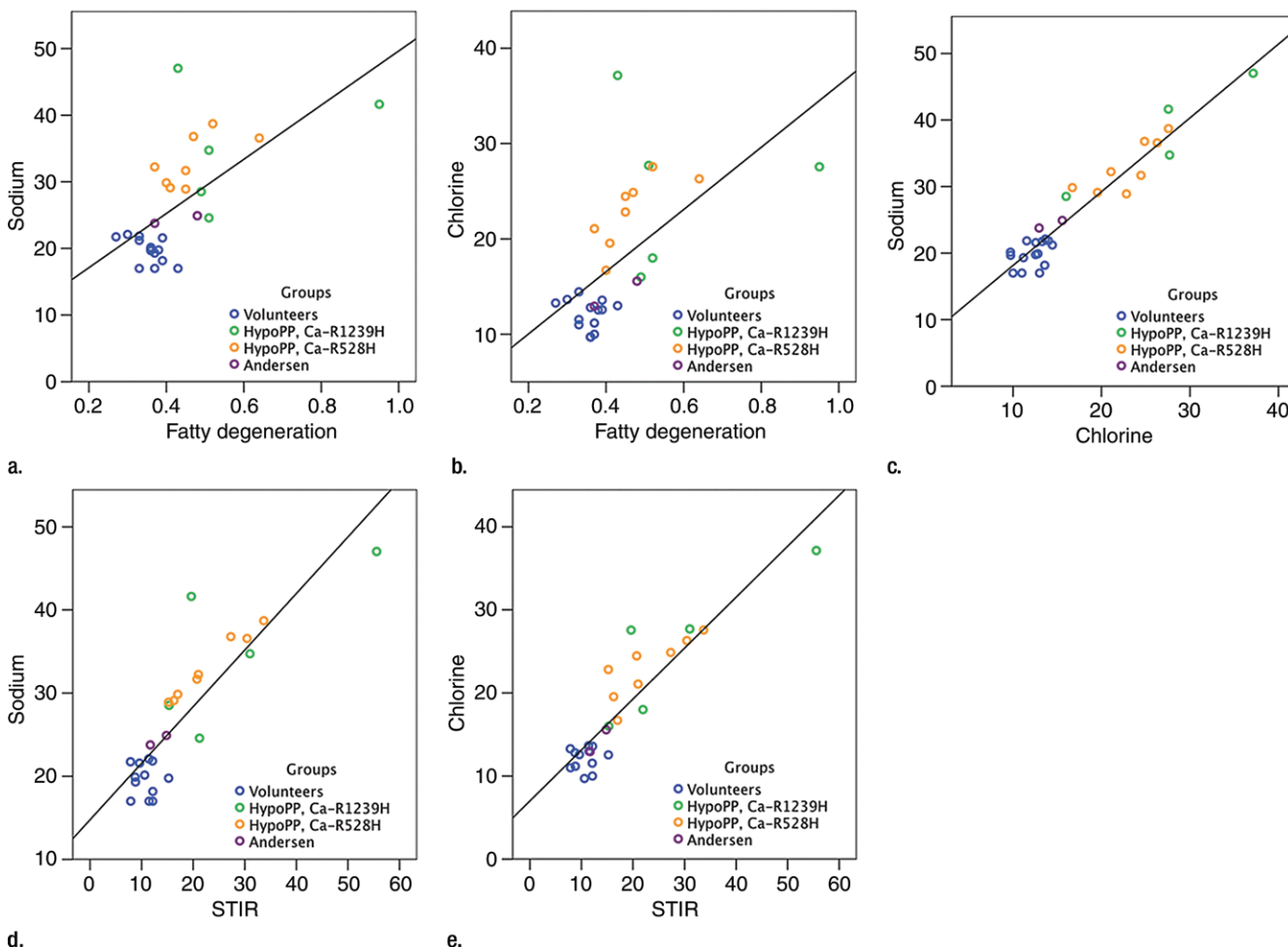


Figure 3: Scatterplots are shown for **(a)** fatty muscular degeneration versus muscular Na⁺ concentration and **(b)** fatty muscular degeneration versus normalized ³⁵Cl SI, as well as **(c)** muscular Na⁺ concentration versus normalized ³⁵Cl SI in the soleus muscle. Scatterplots are shown for **(d)** muscular edema versus muscular Na⁺ concentration and **(e)** muscular edema versus muscular normalized ³⁵Cl SI. Each of the four cohort groups (patients with Cav1.1-R1239H, patients with Cav1.1-R528H, patients with ATS, and healthy volunteers) are represented in different colors.

examined periodic paralysis muscle diseases belong to the category of rare diseases. Moreover, the median age of the control subjects was younger than that of the patients ($P = .03$), given the fact that we examined the volunteers for optimization of the MR imaging protocol and for testing clinical feasibility prior to patient enrollment. In addition, Cl⁻ and sodium experience a biexponential relaxation with a fast component, or T_{2f}^{*}, and a long component, or T_{2L}^{*}, and the short T₂^{*} of ³⁵Cl within healthy muscle tissue (T_{2f}^{*} of 0.37 msec [4]) leads to blurring and to a decrease in effective

spatial resolution. Partial volume correction methods might be applied to enable more accurate quantification (19). However, accurate coregistration of the ¹H MR imaging data would have been required, which was not available in our study. In ³⁵Cl MR imaging of the calf muscles, more than 50% of the signal has already been decayed, although we used an echo time of 0.6 msec to minimize T₂^{*} relaxation weighting (4). Thus, we preferred the use of the term *normalized ³⁵Cl SI* rather than *³⁵Cl concentration*. In the future, imaging of ³⁷Cl instead of ³⁵Cl might enable a more reliable quantification of in vivo

Cl⁻ concentrations at the expense of reduced spatial resolution (20), since ³⁷Cl exhibits an 1.5–1.6-fold longer fast T_{2f}^{*} relaxation time. Also, acquisition techniques that enable even faster signal acquisition, such as sweep imaging with Fourier transformation, might be applied (21,22). Moreover, for clinical applications, a further breakdown into intra- and extracellular Cl⁻ concentrations is desirable. However, a direct means of determining distinct values for the intra- and extracellular Cl⁻ concentrations is not yet available. Therefore, the increased ²³Na and ³⁵Cl SI observed in our study might also, at least

Table 5

Overview of the Muscle Strength of the Lower Extremities

Parameter and Leg	Kir2.1	Cav1.1-R528H	Cav1.1-R1239H
Hip flexion			
Right leg	5 (5–5)	5 (3–5)	4.5 (2–5)
Left leg	5 (5–5)	5 (3–5)	4 (2–5)
Hip extension			
Right leg	5 (5–5)	5 (3–5)	4 (3–5)
Left leg	5 (5–5)	5 (3–5)	3.5 (3–5)
Knee flexion			
Right leg	5 (5–5)	5 (4–5)	4.5 (3–5)
Left leg	5 (5–5)	5 (3–5)	4.5 (2–5)
Knee extension			
Right leg	5 (5–5)	5 (4–5)	4.5 (4–5)
Left leg	5 (5–5)	5 (3–5)	4 (3–5)
Foot plantar flexion			
Right leg	5 (5–5)	5 (5–5)	5 (5–5)
Left leg	5 (5–5)	5 (5–5)	5 (4–5)
Foot dorsiflexion			
Right leg	5 (5–5)	5 (4–5)	5 (5–5)
Left leg	5 (5–5)	5 (4–5)	5 (4–5)

Note.—Results are given as medians, with ranges (minimum to maximum values) in parentheses. For comparison, the median MRC score of all lower leg muscles of the volunteers was 5 (ie, full strength). Muscle strength was evaluated by means of clinical examination and quantified with the aid of the nonlinear grading system defined by the MRC (14).

partially, be caused by an increased extracellular volume fraction (23) instead of exclusive alterations of the cytoplasmic Cl⁻ and Na⁺ concentration.

Once these aforementioned challenges of ³⁵Cl MR imaging are met and the muscular Cl⁻ concentration can be measured more accurately by using ultra-high-field strength MR imaging, the estimation of resting membrane potential of muscle cells can be approximated by using the Nernst equation solely on the basis of MR imaging data. Furthermore, given the fact that the feasibility of potassium 39 imaging of human skeletal muscles with 7-T whole-body MR imaging systems has been demonstrated (24), additional information about the K⁺ ion homeostasis might yield interesting results, particularly for the examined patient population. By using multinuclear and ultra-high-field strength MR imaging techniques in patients with periodic paralysis, monitoring of disease progression and therapy may be more precisely possible than it would be by using conventional proton MR imaging. Also, multinuclear

MR imaging demonstrates more information about mutation-dependent alterations of muscle pathophysiology in muscular periodic paralysis, such as differences in Cl⁻ and Na⁺ homeostasis, reflecting pathologic cellular ion currents that could not be visualized in conventional proton MR imaging.

In summary, by using 7-T MR imaging, changes of Na⁺ and Cl⁻ homeostasis can be visualized in periodic paralysis and are most pronounced in the severe phenotype Cav1.1-R1239H, which manifests almost daily paralytic episodes. Regarding clinical relevance, 7-T ²³Na and ³⁵Cl MR imaging can be used to monitor myocellular ion homeostasis noninvasively in a clinically feasible acquisition time and may be of help in testing for pathogenesis, estimating prognosis, and monitoring treatment in periodic paralysis.

Acknowledgments: We are grateful to the volunteers, as well as the patients and their families, for their participation.

Disclosures of Conflicts of Interest: M.A.W. disclosed no relevant relationships. A.M.N. dis-

closed no relevant relationships. A.M.M. disclosed no relevant relationships. P.G. disclosed no relevant relationships. K.J.R. disclosed no relevant relationships. M.B.W. disclosed no relevant relationships. M.E.L. disclosed no relevant relationships. H.P.S. disclosed no relevant relationships. H.U.K. Activities related to the present article: disclosed no relevant relationships. Activities not related to the present article: author received grants, nonfinancial support (hardware and software), and payment from Siemens for board membership and serving on speakers' bureaus; author received grants and payment from Boehringer Ingelheim for educational presentations and serving on speakers' bureaus; author received nonfinancial payment (provision of consumables) and payment from Bayer for serving on speakers' bureaus; author received payment from Novartis, Almirall, and GSK for serving on speakers' bureaus. Other relationships: disclosed no relevant relationships. F.L.H. disclosed no relevant relationships.

References

1. Statland JM, Barohn RJ. Muscle channelopathies: the nondystrophic myotonias and periodic paralysis. *Continuum (Minneapolis)* 2013;19(6 Muscle Disease):1598–1614.
2. Jurkat-Rott K, Weber MA, Fauler M, et al. K⁺-dependent paradoxical membrane depolarization and Na⁺ overload, major and reversible contributors to weakness by ion channel leaks. *Proc Natl Acad Sci U S A* 2009;106(10):4036–4041.
3. Tristani-Firouzi M, Etheridge SP. Kir 2.1 channelopathies: the Andersen-Tawil syndrome. *Pflugers Arch* 2010;460(2):289–294.
4. Nagel AM, Lehmann-Horn F, Weber MA, et al. In vivo ³⁵Cl MR imaging in humans: a feasibility study. *Radiology* 2014; 271(2):585–595.
5. Nagel AM, Amarteifio E, Lehmann-Horn F, et al. 3 Tesla sodium inversion recovery magnetic resonance imaging allows for improved visualization of intracellular sodium content changes in muscular channelopathies. *Invest Radiol* 2011;46(12):759–766.
6. Koch MC, Steinmeyer K, Lorenz C, et al. The skeletal muscle chloride channel in dominant and recessive human myotonia. *Science* 1992;257(5071):797–800.
7. Lehmann-Horn F, Jurkat-Rott K. Voltage-gated ion channels and hereditary disease. *Physiol Rev* 1999;79(4):1317–1372.
8. Insko EK, Bolinger L. Mapping of the radiofrequency field. *J Magn Reson A* 1993; 103(1):82–85.
9. Olsen DB, Gideon P, Jeppesen TD, Vissing J. Leg muscle involvement in facioscapulo-

- humeral muscular dystrophy assessed by MRI. *J Neurol* 2006;253(11):1437–1441.
10. Weber MA, Nagel AM, Wolf MB, et al. Permanent muscular sodium overload and persistent muscle edema in Duchenne muscular dystrophy: a possible contributor of progressive muscle degeneration. *J Neurol* 2012; 259(11):2385–2392.
 11. Marden FA, Connolly AM, Siegel MJ, Rubin DA. Compositional analysis of muscle in boys with Duchenne muscular dystrophy using MR imaging. *Skeletal Radiol* 2005;34(3):140–148.
 12. Nagel AM, Lanz T, Berthel D, Resmer F, Semmler W, Umatham R. A measurement setup for combined chlorine (³⁵Cl) and sodium (²³Na) MRI of the human brain [abstr]. In: *Proceedings of the Twenty-First Meeting of the International Society for Magnetic Resonance in Medicine*. Berkeley, Calif: International Society for Magnetic Resonance in Medicine, 2013; 1984.
 13. Nagel AM, Laun FB, Weber MA, Matthies C, Semmler W, Schad LR. Sodium MRI using a density-adapted 3D radial acquisition technique. *Magn Reson Med* 2009;62(6): 1565–1573.
 14. Dyck PJ, Boes CJ, Mulder D, et al. History of standard scoring, notation, and summation of neuromuscular signs. A current survey and recommendation. *J Peripher Nerv Syst* 2005;10(2):158–173.
 15. Nguyen HL, Pieper GH, Wilders R. Andersen-Tawil syndrome: clinical and molecular aspects. *Int J Cardiol* 2013;170(1):1–16.
 16. Kirsch S, Augath M, Seiffge D, Schilling L, Schad LR. In vivo chlorine-35, sodium-23 and proton magnetic resonance imaging of the rat brain. *NMR Biomed* 2010;23(6):592–600.
 17. Baier S, Krämer P, Grudzinski S, Fatar M, Kirsch S, Schad LR. Chlorine and sodium chemical shift imaging during acute stroke in a rat model at 9.4 Tesla. *MAGMA* 2014;27(1):71–79.
 18. Schepkin VD, Elumalai M, Kitchen JA, Qian C, Gor'kov PL, Brey WW. In vivo chlorine and sodium MRI of rat brain at 21.1 T. *MAGMA* 2014;27(1):63–70.
 19. Niesporek SC, Hoffmann SH, Berger MC, et al. Partial volume correction for in vivo (²³Na)-MRI data of the human brain. *Neuroimage* 2015;112:353–363.
 20. Schork J, Kollefrath A, Roesler MB, Umatham R, Nagel AM. In vivo ³⁷Cl MRI of human calf muscle at 7T [abstr]. In: *Proceedings of the Twenty-Third Meeting of the International Society for Magnetic Resonance in Medicine*. Berkeley, Calif: International Society for Magnetic Resonance in Medicine, 2015; 756.
 21. Idiyatullin D, Corum C, Park JY, Garwood M. Fast and quiet MRI using a swept radio-frequency. *J Magn Reson* 2006;181(2):342–349.
 22. Idiyatullin D, Suddarth S, Corum CA, Adriany G, Garwood M. Continuous SWIFT. *J Magn Reson* 2012;220:26–31.
 23. Donahue KM, Weisskoff RM, Parmelee DJ, et al. Dynamic Gd-DTPA enhanced MRI measurement of tissue cell volume fraction. *Magn Reson Med* 1995;34(3):423–432.
 24. Umatham R, Rösler MB, Nagel AM. In vivo ³⁹K MR imaging of human muscle and brain. *Radiology* 2013;269(2):569–576.